Experiments in Fluids (2025) 66:44
https://doi.org/10.1007/s00348-024-03942-6

RESEARCH ARTICLE

Splashing correlation for single droplets impacting liquid films under non-isothermal conditions

Daniel Vasconcelos[1] · Jorge Barata[1] · André Silva[1]

Received: 21 August 2024 / Revised: 9 December 2024 / Accepted: 10 December 2024 / Published online: 7 February 2025

Abstract

The droplet impact phenomenon onto liquid films is predominant in a variety of modern industrial applications, including internal combustion engines and cooling of electronic devices. These are characterised by heat and mass transfer processes, such as evaporation, condensation and boiling. However, studies regarding droplets and liquid films under non-isothermal conditions are scarce in the literature and do not explore temperature-dependent phenomena. Due to this, the main objective of this work is to evaluate the influence of temperature on the splashing occurrence of single droplets impinging onto liquid films under the presence of a heat flux. The crown evolution is evaluated qualitatively to provide insight regarding breakup mechanisms. Water, n-heptane and n-decane are the fluids considered for the current study, as these provide a wide range of thermophysical properties and saturation temperatures. The splashing dynamics are evaluated by varying the droplet impact velocity and dimensionless temperature of the liquid film. Qualitative results show that an increase in the liquid film temperature leads to the transition from spreading to splashing, which is less evident for fuels in comparison with water. For water and n-heptane, the formation of cusps on the crown rim is promoted, which is associated with ligament breakup. For n-decane, the crown rims are relatively homogeneous in terms of shape and size, whereas the atomisation process varies a function of the liquid film temperature. Visually, the secondary droplets exhibit a greater size in comparison with lower temperatures. Transitional regimes display some irregularities, such as splashing suppression/reduction, which require further attention. In terms of splashing correlation, the authors propose to develop a non-splash/splash boundary for both iso- and non-isothermal conditions. Results show that the splashing threshold is dependent on the thermophysical properties and the dimensionless temperature of the liquid film.

List of symbols

D_c	Borosilicate glass cylinder inner diameter [cm]
D_d	Droplet impact diameter [mm]
e_c	Borosilicate glass cylinder thickness [cm]
h	Liquid film thickness [mm]
h^*	Dimensionless liquid film thickness [−]
K	Splashing threshold parameter [−]
Oh	Ohnesorge Number [−]
p	Splashing occurrence probability [−]
q	Heat flux $\left[\mathrm{W/m^2}\right]$
Re	Reynolds Number [−]
T	Temperature [°C]
t	Time [s]
U_d	Droplet impact velocity $\left[\mathrm{m/s}\right]$
We	Weber Number [−]

Greek Symbols

μ	Dynamic viscosity $\left[\mathrm{mPa/s}\right]$
ρ	Density $\left[\mathrm{kg/m^3}\right]$
σ	Surface tension $\left[\mathrm{mN/m}\right]$
τ	Dimensionless time [−]
θ	Dimensionless temperature [−]

Subscripts

air	Surrounding air
arit	Arithmetic
d	Droplet
f	Liquid film
geom	Geometric
h	Horizontal
rel	Release

✉ Daniel Vasconcelos
daniel.vasconcelos.rodrigues@ubi.pt

Jorge Barata
jbarata@ubi.pt

André Silva
andre@ubi.pt

[1] AEROG, Aeronautics and Astronautics Research Center, LAETA, University of Beira Interior, Covilhã, Portugal

sat Saturation point
v Vertical

1 Background

Splashing is an intriguing phenomenon in fluid mechanics. In the context of droplet impact, this term can be defined by the detachment of secondary droplets throughout the development of the outcome. This is associated with the Rayleigh-Plateau capillary instability (Plateau 1873; Rayleigh 1879), which is the main mechanism for liquid jet breakup. Low energy outcomes usually develop into spreading, rebound and coalescence (Bai, Gosman 1995). These are characterised by simple topological structures, where the main droplet smoothly advances onto the substrate until reaching stability. An increase in the system entropy through means of increasing kinetic and thermal effects leads to more complex topology changes, such as splashing.

The droplet impact phenomena is predominant in a variety of modern and industrial applications. Internal combustion engines with direct fuel injection (Panão and Moreira 2005), spray cooling (Jia and Qiu 2003), heat exchangers (Šikalo and Ganić 2006) and ink-jet printing (Van Dam and Le Clerc 2004) are several examples of which liquid films play a major role in the underlying dynamics. Controlling the impact outcome is crucial depending on the application, as spreading is desired for spray coatings and ink-jet printers, whereas splashing improves both the mixing and evaporation in combustion processes (Josserand et al. 2016). The Weber number, $We = \rho U_d^2 D_d/\sigma$, the Reynolds number, $Re = \rho U_d D_d/\mu$, and the Ohnesorge number, $Oh = \mu/\sqrt{\rho\sigma D_d}$, are examples of dimensionless numbers that define multiphase flows involving impacting droplets (Yarin 2006), where ρ is density, D_d and U_d are the droplet impact diameter and velocity, respectively, σ is the surface tension, and μ is the viscosity. In the presence of wetted surfaces, the dimensionless thickness, $h^* = h/D_d$, distinguishes the liquid film regimes based on its dependency with the surface properties (Tropea, Marengo 1999). These parameters have been investigated in several studies, including surface morphology (Foltyn et al. 2021), two-phase flow dynamics (Ferrão et al. 2020), heat and mass transfer processes (Liang et al. 2019), combustion (Ferrao et al. 2021), among others. For spray impingement systems, the formation of liquid films due to poor atomisation and/or vaporisation in internal combustion engines results in unburned hydrocarbons and particle emissions (Moreira et al. 2010). Comprehending the underlying mechanisms associated with secondary atomisation is crucial to improve the efficiency of internal combustion engines in terms of increasing energy production and reducing pollutant emissions. Similarly, for applications involving highly density heat fluxes, such as spray cooling, the interactions between the heated surface and the impinging droplets are extremely important (Selvam et al. 2006). These are characterised by conduction and convection as well as phase change, leading to the nucleation of vapour bubbles. Determining the governing parameters for applications involving multiphase heat transfer is extremely difficult due to the complexity of the physical system, requiring further analysis.

Extensive research has been performed regarding influencing parameters on the splashing phenomena. Cossali et al. (1997) identified two splashing mechanisms based on the Ohnesorge number: prompt and delayed/crown splash. Prompt splash is associated with low viscosity values, and refers to the release of secondary droplets at early stages of the outcome, whereas crown splash occurs when the crown fully develops, which is related to later stages. Vander Wal et al. (2006b) studied impacting droplets onto liquid films of variable thickness for water, n-heptane and methanol. Both prompt and crown splashing are visualised for the lower thicknesses, $0.1 < h^* < 1$. An increase in the liquid film thickness restricts and inhibits prompt and crown splash, respectively, as the impact energy dissipates onto the liquid film rather than into the crown formation and posterior secondary atomisation. Viscosity has an opposite effect for dry and liquid film surfaces, promoting splashing on the dry surface and inhibiting it on wetted surfaces. Higher values of surface tension suppress the splashing phenomenon, regardless of the impacting surface. Rougher surfaces lower the splashing threshold and affect the splashing dynamics (Vander Wal et al. 2006a). Wang and Chen (2000) stated that, for extremely thin liquid films ($h^* < 0.1$), the critical Weber number for the onset of splashing is independent of the liquid film thickness. Liang et al. (2014) studied the effect of gas density and viscosity on the crown development. Decreasing liquid–gas viscosity ratios lead to the suppression of the splashing phenomenon, whereas the density ratios mainly affect the crown curvature.

In order to comprehend the role of each of these properties on the mechanisms of splashing, several authors investigated the conditions required for splashing to occur. The splashing threshold parameter, K, was defined to account for the different variables that characterise the phenomena. As previously discussed, viscosity and surface tension display a strong influence on the splashing threshold (Rioboo et al. 2003). This means that the non-splash/splash boundaries are dependent on viscous and surface tension forces, which translate to the Weber, Reynolds and Ohnesorge numbers. Table 1 displays the existing correlations for the non-splash/splash boundaries presented in the literature. Yarin and Weiss (1995) quantitatively studied the splashing phenomenon, taking into account these properties in addition to surface temperature and roughness, droplet impact diameter and velocity, among others. The threshold was defined in terms

Table 1 Review of the existing correlations for non-splash/splash thresholds for single droplet impact onto a liquid film

Author(s)	Experimental conditions	Correlation(s)
Yarin and Weiss (1995)	$U_d < 30$ m/s $D_d = 70 - 340$ µm	$K = WeOh^{-0.4} = 2400$
Cossali et al. (1997)	$We = 200 - 1600$ $Oh = 2.2e-3 - 1.41e-1$ $h^* = 0.08 - 1.2$	$K = WeOh^{-0.4} = 2100 + 5880h^{*1.44}$
Han et al. (2000)	$We = 200 - 1600$ $Oh = 2.2e-3 - 1.41e-1$ $h^* = 0.08 - 1.2$	$K = \left(1500 + \frac{650}{R_a^{0.42}}\right)\left[1 + 0.1Re_n^{0.5}\ \min(\delta, 0.5)\right]$
Vander Wal et al. (2006c)	$We = 127 - 1200$ $Re = 988 - 1.39e4$ $Oh = 2.49e-3 - 6.51e-2$ $h^* = 0.1 - 10$	$K = OhRe^{1.17} = 63$
Huang and Zhang (2008)	$log(We) = 0.3 - 3.4$ $log(Re) = 1.5 - 3.9$ $h^* = 0.3 - 1.3$	$K = (WeRe)^{0.25} = 25 + 78^{1.44}$
Gao and Li (2015)	$D_d = 2.6 - 4.6$ mm $U_d = 0.63 - 4.2$ m/s $h^*U_f^* = 0.05 - 0.18$	$K = WeRe^{0.5}\left(1 + \bar{h}_f\bar{U}_f^2\right)\left(1 + \bar{h}_f\bar{U}_f\right)^{1/2} = 3378$

of the Capillary number, which can be formulated as a function of the Weber and Ohnesorge numbers. This is a standard approach in terms of the splashing mechanism, as explored by different authors (Rioboo et al. 2003; Okawa et al. 2006). Cossali et al. (1997) developed an empirical correlation as a function of the liquid film and surface roughness. Opposite to Yarin and Weiss (1995); Cossali et al. (1997) stated that the splashing threshold parameter is dependent on the liquid film thickness, requiring more impact energy for splashing to occur for thicker liquid films. Han et al. (2000) adapted the correlation of Cossali et al. (1997), proposing an alternative to reduce the effect of liquid film thickness, and implementing the surface roughness directly onto the formulation of the splashing threshold parameter. Vander Wal et al. (2006c) display the correlation in a different form, which is based on the Reynolds and Ohnesorge numbers, similar to Mundo et al. (1995). Most recently, the splashing thresholds have been improved to account for more complex dynamics of the impact phenomena. Gao and Li (2015) investigated this topic for flowing films, in which the splashing threshold is also dependent on the liquid film average thickness and velocity. An increase in these parameters leads to a lower threshold, thereby inducing splashing at lower values of the Weber and Reynolds numbers. Okawa et al. (2021) and Zhu et al. (2021) categorised the prompt and crown splashing outcomes as two separate occurrences in the splashing mechanism, requiring different thresholds for each instance.

Despite the extensive work regarding single droplets impacting liquid films and associated splashing regimes, these are limited to isothermal conditions. In modern applications, such as internal combustion engines and electronic cooling devices, heat and mass transfer processes are predominant which, in two-phase flows, correspond to evaporation, condensation and boiling. Introducing the impact of temperature on interfacial dynamics and breakup mechanisms is essential to narrow the gap between single droplet studies and industrial applications. The main objective of this work is to evaluate the influence of liquid film temperature on splashing mechanisms of single droplets impinging onto heated liquid films. The splashing occurrence is analysed for a wide range of experimental conditions, including different fluids, impact velocities and liquid film temperatures. The crown evolution is evaluated qualitatively to provide insight regarding breakup mechanisms. The experimental results are evaluated against the existing correlations in the literature, and a non-splash/splash correlation is developed for both iso- and non-isothermal conditions.

2 Experimental setup

Figure 1 illustrates the schematic of the experimental setup. It is divided into several components, including the heating system, imaging equipment and associated illumination setup, pumping system and impact surface. The droplet dispensing system consists of two NE-1000 syringe pumps connected through tubes to hypodermic needles. Imposing a specific flow rate on the syringe pump pushes the fluid until reaching the needle. A droplet is slowly formed on the tip of the hypodermic needle until reaching a critical size, entering a free fall motion. The main syringe pump is aligned with the centre of the impact surface for outcome visualisation, and the secondary pump is employed to account for the fluid evaporation rate, which is associated with the liquid film thickness variation. The droplet impinges onto a stationary liquid film supported by

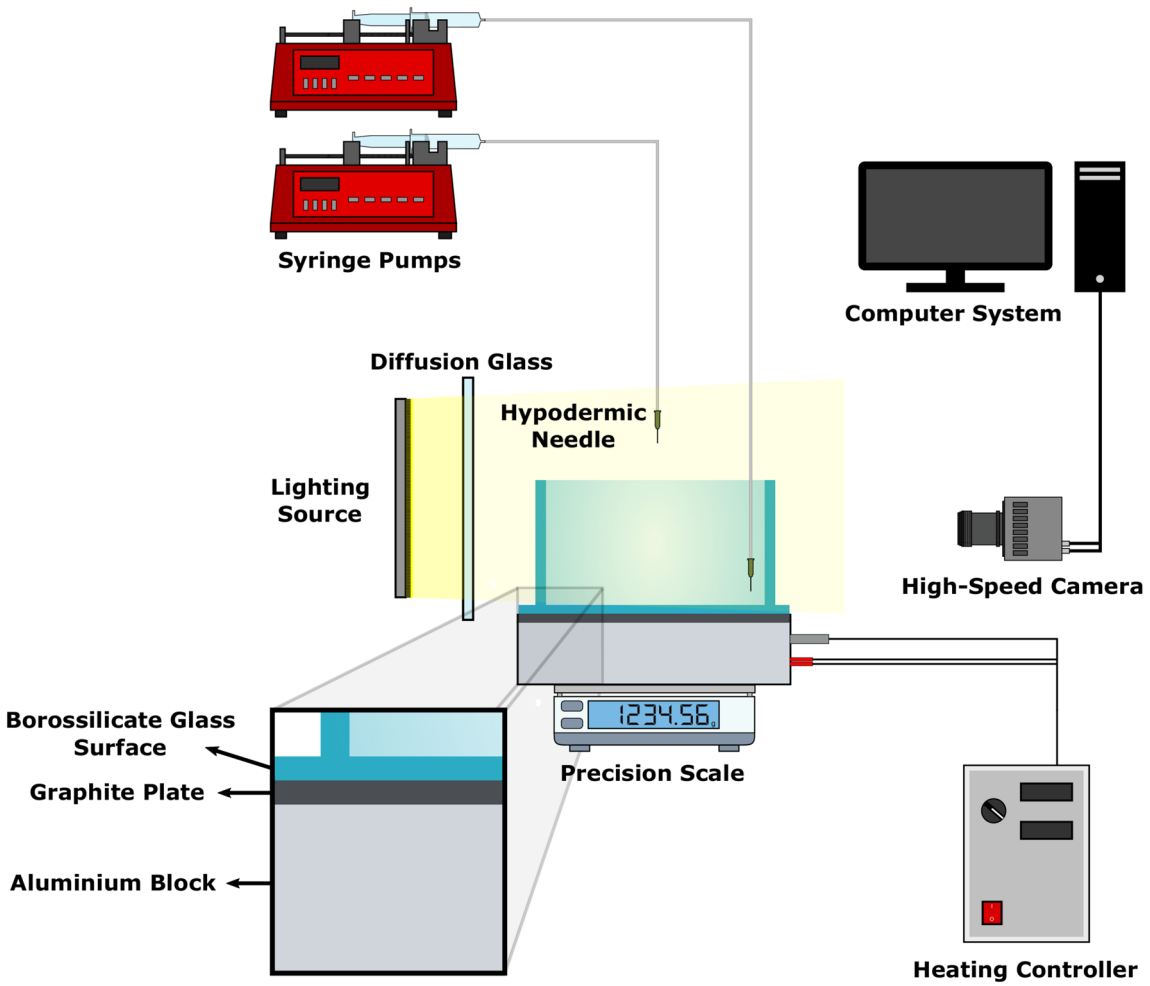

Fig. 1 Schematic of the experimental setup (Vasconcelos et al. 2023)

a borosilicate glass container. This material was the most optimal choice in terms of optical and thermal properties, coupled with affordability and accessibility for manufacture. The container is a two-part surface consisting of a glass plate of dimensions 15 cm × 15 cm × 0.2 cm and a hollow cylinder with an internal diameter of $D_c = 12$ cm and a thickness of $e_c = 0.5$ cm. These are attached by a bonding agent, LOCTITE SI 5366, in order to prevent fluid leakage from the contact area. This borosilicate glass surface is positioned over an aluminium block that acts as a heat source in order to heat the liquid film by conduction. The heating system is composed of a heating device connected to an aluminium block with 4 embedded cartridge heaters of 250 W each, providing a local heat source. The temperature imposed on the impact surface is controlled by an embedded type-k thermocouple 0.75 cm below the aluminium surface. A graphite plate is positioned amidst the aluminium block and the glass container to block incoming reflections from the illumination setup, which affects high-speed imaging.

In terms of image acquisition, the droplet impact phenomena is captured by a Photron FASTCAM mini UX50 high-speed digital camera coupled with a Macro Lens Tokina AT-X M100 AF PRO D to achieve higher spatial resolutions. A frame rate of 4000 fps and a shutter speed of 1/25000 s were employed for the phenomena recording. The imaging setup is connected to a local computer for data storage and post-processing. Opposed to the high-speed camera, a 20 W lamp supplies a light-focused source which passes through a diffusion glass, providing uniform lighting on the impact phenomena. Additionally, a precision scale is employed for the liquid film weight measurements to account for weight loss due to evaporation.

Figure 2 displays the physical setup regarding the impact phenomena. A single droplet of diameter D_d and impact velocity U_d impinges onto a static liquid film of thickness h. The liquid film is continuously affected by a heat flux q, increasing its temperature by conduction. The droplet is released from the hypodermic needle at room temperature, $T_d = T_{air}$. Due to the non-isothermal

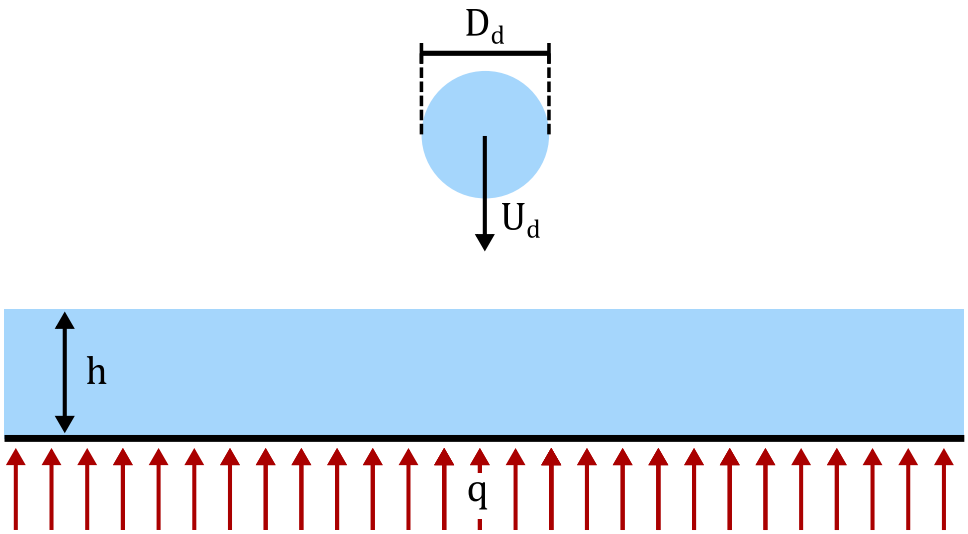

Fig. 2 Schematic of a droplet impinging onto a liquid film affected by a heat flux. Adapted from Vasconcelos et al. (2023)

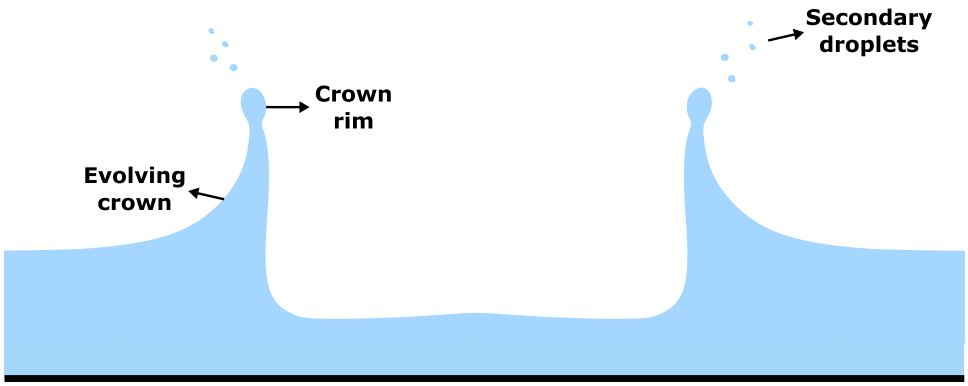

Fig. 3 Schematic of a developing crown and secondary atomisation following the impact of a single droplet impinging onto a liquid film

conditions, the liquid film dimensionless temperature, $\theta = \left(T_f - T_{air}\right)/\left(T_{sat} - T_{air}\right)$, is adopted for the current work. This parameter characterises the impact regime based on the liquid film temperature, T_f, the saturation temperature of the fluid, T_{sat}, and the ambient temperature, T_{air}. The dimensionless temperature is limited between $\theta = 0$ and $\theta = 1$ for the current setup, where $\theta = 0$ corresponds to isothermal conditions $\left(T_f = T_{air}\right)$, and $\theta = 1$ to the liquid film boiling point $\left(T_f = T_{sat}\right)$. Liquid film temperatures below ambient temperatures would require adapting the experimental setup by implementing a cooler as a heat sink. For regimes above the saturation temperature, the liquid film becomes unstable, as increased heat fluxes contribute to a more chaotic boiling phenomenon, potentially resulting in the liquid film rapid evaporation (Vasconcelos et al. 2024). The operating range is limited by the bonding agent of the borosilicate glass container, which is capable of maintaining structural integrity up to operating temperatures of $T = 250$ °C. Subsequent to impact, for higher energy impacts, a liquid crown emerges from the liquid film, possibly originating secondary atomisation from the crown rim, as can be identified in Fig. 3. These outcomes are typically associated with breakup mechanisms.

Table 2 Thermophysical properties of water, n-decane and n-heptane at room temperature (T_{air}=20 °C)

Fluid	ρ [kg/m^3]	μ [mPa s]	σ [mN/m]	T_{sat} [°C]
Water	998.2	1.002	72.73	99.8
N-heptane	685.8	0.412	20.29	98.4
N-decane	732.1	0.929	23.89	174.1

For later stages, the evolving crown disintegrates, merging back with the liquid film until reaching a stable condition.

Table 2 displays the fluids utilised in the current study. These were selected based on differences in thermophysical properties and saturation temperatures, allowing for a wider range of experimental conditions. Water displays higher values of viscosity and surface tension in comparison with fuels and is an extensively researched fluid in the literature (Ersoy and Eslamian 2020; Yu et al. 2022). N-decane and n-heptane are fuels with low surface tension, where n-decane exhibits a higher saturation temperature and viscosity. These are surrogate fuels for kerosene/jet-fuel (Raza et al. 2019; Le et al. 2023) and diesel (Farrell et al. 2007), respectively. The

thermophysical properties are temperature dependent, and the correspondent correlations are displayed in appendix A and in the literature (Dinçer and Zamfirescu 2016; Yaws 1999). Several other fluids were initially considered, such as jet fuel, biofuel and mixtures, however several constraints emerged relative to the saturation temperatures exceeding the maximum operating conditions and the multicomponent nature of the fuels. The latter relates to each component of the fluid having different saturation points and evaporation rates. When subjected to a constant heat flux, the thermophysical properties are not only dependent on temperature, but also on the mass fraction of each of the components, significantly increasing the difficulty in quantifying the liquid film properties. These reasons led to disregarding jet fuel, biofuel and mixtures as operating fluids for the current experimental setup.

In terms of impact conditions, air temperature and relative humidity are maintained at 20°C ± 2°C and 50% ± 3%, respectively. Preliminary studies involve the droplet diameter and impact velocity measurements in order to quantify the impact phenomena. The droplet diameter is calculated by averaging the horizontal and vertical diameters during free fall. Figure 4 exhibits the horizontal, D_h, and vertical, D_v, diameter measurements for an n-heptane droplet during free fall as a function of the droplet release time, t_{rel}, where $t_{rel} = 0$ ms corresponds to the instant the droplet detaches from the needle. Consequently, two averaging diameters were calculated based on these measurements, including an arithmetic average, $D_{arit} = (D_h + D_v)/2$, and a geometric average diameter, $D_{geom} = (D_h^2 D_v)^{1/3}$. It is possible to visualise that both the arithmetic and geometric averaging diameters display similar measurements. However, the geometric averaging presents a higher standard deviation in comparison

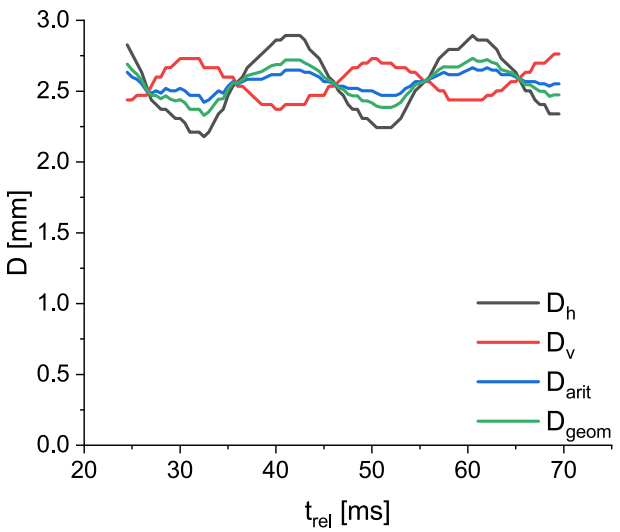

Fig. 4 Analysis of horizontal, vertical, arithmetic and geometric diameters for different instants during the droplet free fall

with the arithmetic averaging, $D_{arit} = 2.56 \pm 0.06$ mm and $D_{geom} = 2.55 \pm 0.11$ mm. Similar tendencies were visualised for water and n-decane. Due to this, the arithmetic average diameter was adopted to the current study.

In contrast, the impact velocity is defined by the vertical difference of centroids of the last frame before impact and successive prior frames. These parameters are analysed through a MATLAB algorithm, consisting of background subtraction, binarisation and droplet detection. Similarly, the liquid film must also be assessed in terms of temperature and evaporation rates (due to the presence of a heat flux). The former can be obtained by immersing several type-k thermocouples in the liquid film, and conducting temperature measurements over extended periods of time for a preselected temperature on the heating device. These were executed for approximately 30 min after reaching a stabilisation temperature, as the initial heating phase consists of heating the liquid film from ambient temperature until reaching a steady condition. The temperature measurements were performed at a vertical distance of 0.10 ± 0.05 mm from the borosilicate glass surface. The uncertainties for temperature measurements were calculated based on the mean average and standard deviation temperatures during the stabilisation phase. For the evaporation rate, a precision scale is adopted to account for mass variations by weighing the liquid film periodically when it reaches a constant temperature. This is a similar approach to maintaining a constant liquid film thickness throughout the experiments. Once the liquid film temperature stabilises succeeding the heating phase, the liquid film is weighted, corresponding to a specific film thickness. If this value exceeds a certain threshold, meaning a higher liquid film thickness, fluid is removed, either manually or through evaporation, until reaching an acceptable range. On the contrary, if the measured value is below the threshold (due to constant fluid evaporation), fluid is added to the liquid film. The second syringe pump ensures a stable liquid film thickness throughout the experiments. The fluid is added near the radial walls to avoid temperature gradients between these regions. Additionally, a short period of time is required to guarantee the liquid film temperature stabilisation, followed by the re-evaluation of the liquid film weight. A more detailed description of the experimental procedure and methodology, including the temperature and evaporation rate measurements, is presented in a previous work (Vasconcelos et al. 2023).

The experimental conditions considered for the different fluids are represented in Table 3. The splashing dynamics are evaluated by mainly varying the droplet impact velocity and dimensionless temperature of the liquid film. The considered values range from non-splash to splash conditions, therefore providing insight onto the different regimes. The splashing is characterised by the formation of secondary droplets, whereas spreading displays a smooth crown development

Table 3 Experimental conditions for the different fluids

Fluid	D_d [mm]	U_d [m/s]	h^*	θ
Water	2.67	1.88 – 2.71	1.0	0 – 0.75
N-heptane	2.56	1.23 – 2.09	1.0	0 – 0.81
N-decane	2.72	1.40 – 2.21	1.0	0 – 0.82

with no associated breakup. A single droplet diameter was established for each of the fluids, corresponding to a constant liquid film thickness. In terms of the droplet geometrical parameters, the errors related to the impact diameter and velocity measurements are within an acceptable range, displaying a maximum relative error of 2.6% and 0.72%, respectively. Similarly, the maximum relative error associated with the temperature measurements is 3.12% for water, 0.45% for n-heptane and 0.43% for n-decane. Regarding the total sample size, different authors consider between 3 to 5 impinging droplets for non-heated liquid films (Manzello and Yang 2002; Castillo-Orozco et al. 2015). In order to guarantee repeatability and consistency of the impact outcomes, due to the instabilities associated with the splashing phenomenon and the influence of temperature, and following previous works (Vasconcelos et al. 2023; Ribeiro et al. 2023), a minimum of 10 droplets is evaluated for each experimental condition. This number may increase for transitional regimes, such as non-splash/splash boundaries. The pixel size was varied between 26.0 µm and 29.4 µm.

3 Results and discussion

The qualitative and quantitative analyses are performed with the objective of understanding the impact of temperature on the droplet impact phenomena. These are divided into splashing dynamics and overall crown evolution, and the splashing probability and consequent non-splash/splash correlation, respectively. The splashing occurrence probability is characterised as the ratio of the number of impacting outcomes that result in secondary atomisation to the number of impacting droplets. Both prompt and crown splashing are considered for the splashing occurrence probability. This is verified for each experimental condition for a minimum of 10 impacting droplets due to the instabilities associated with the breakup mechanisms. These results are obtained through visualisation of the impact phenomena. Table 4 exhibits the probability related to the occurrence of splashing for the water droplet impact onto a liquid film. The italic text represents splashing, which occurs for a probability of $p > 70\%$, the bold text relates to spreading with a probability of $p < 30\%$, and the bold italic text is the transition regime ($30\% \leq p \leq 70\%$). Both isothermal ($\theta = 0$) and non-isothermal ($\theta > 0$) conditions are considered for the probability analysis. For non-heated liquid films, an increase in the impact velocity leads to the transition from spreading to splashing. These are within the non-splash/splash boundaries defined by Vander Wal et al. (2006c). In terms of liquid film temperature, for transitional regimes $\left(2.19\ \text{m/s} \leq U_d \leq 2.42\ \text{m/s}\right)$, an increase in the dimensionless temperature leads to an increase in the splashing probability, transitioning from $p = 0\%$ for $\theta = 0$ and $\theta = 0.11$, to $p > 90\%$ for $\theta = 0.44$. Outer regimes ($U_d = 1.88$ m/s and $U_d = 2.71$ m/s) do not display a significant variation in the splashing occurrence. However, for $U_d = 2.71$ m/s, higher liquid film temperatures generate more secondary droplets, which is associated with lower values of surface tension and viscosity. Several discrepancies are spotted in the boundaries of the spread/splashing phenomenon, in which an increase in the impact velocity and/or dimensionless temperature may result in a decrease of splashing. For $\theta = 0.23$, increasing the impact velocity from $U_d = 2.29$ m/s to $U_d = 2.42$ m/s causes a sudden decrease in the splashing occurrence percentage from $p = 90\%$ to $p = 10\%$. This tendency is similar in certain regions by increasing the dimensionless temperature, as presented for $U_d = 2.42$ m/s. This condition displays a slight decrease in the splashing occurrence from $p = 100\%$ to $p = 64\%$ when increasing the liquid film dimensionless temperature from $\theta = 0.44$ to $\theta = 0.60$, respectively.

In order to comprehend these irregularities in the regime maps, Fig. 5 exhibits the visualisation of the water droplet

Table 4 Splashing occurrence percentage as a function of the impact velocity and dimensionless temperature for water

Impact velocity[m/s]						
θ	1.88	2.11	2.19	2.29	2.42	2.71
0	**0**	**0**	**0**	**0**	**0**	*100*
0.11	**0**	**0**	**0**	**0**	**0**	*100*
0.23	**0**	**0**	***38.5***	*90*	**10**	*100*
0.44	**0**	**0**	*90*	*100*	*100*	*100*
0.60	**0**	**30**	*100*	*80*	***64***	*100*
0.75	**10**	**10**	*100*	*90*	*80*	*100*

Spreading - Bold, Transition - Bold Italic, Splashing - Italic

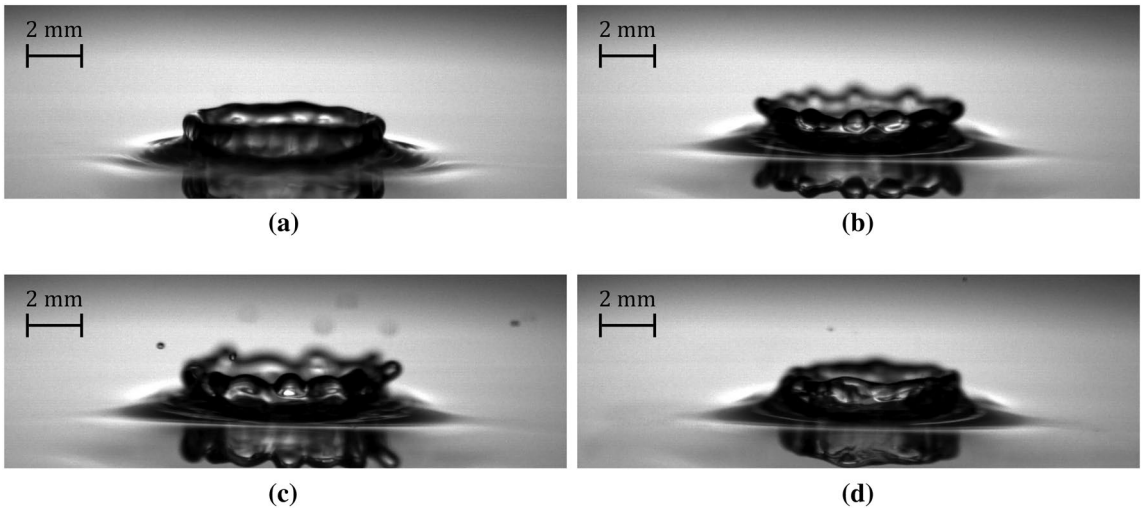

Fig. 5 Visualisation of the impact phenomena of a water droplet onto a liquid film for different temperatures $\left(U_d = 2.42\ \text{m/s},\ D_d = 2.67\ \text{mm}\right)$: a) $\theta = 0$, $\tau = 2.72$; b) $\theta = 0.23$, $\tau = 2.27$; c) $\theta = 0.44$, $\tau = 2.72$; d) $\theta = 0.60$, $\tau = 2.49$

impact onto a liquid film for varying liquid film temperatures. For $\theta = 0$, no formation of secondary droplets is verified, and the crown develops rather smoothly with no formation of cusps in the crown rim. The evolving crown reaches its maximum height, followed by a continuous decrease until merging with the liquid film. For $\theta = 0.23$, instabilities arise on the developing crown, which are denominated as fingers/cusps. These are typically associated with secondary atomisation, as these structures tend to experience both stretching and thinning, which may lead to its breakup, resulting in the release of secondary droplets. For this condition, the cusps developed in the crown rim do not breakup, meaning that no secondary atomisation occurs. For $\theta = 0.44$, these structures reach a critical thickness, leading to its breakup and originating secondary droplets. The crown displays a more irregular shape, which is also a result of liquid ligament breakup. The regime transition from spreading to splashing is due to the thermophysical properties, such as density, viscosity, and surface tension, decreasing with temperature. This is in accordance with the splashing correlations presented in Table 1, as lower values of viscosity and surface tension contribute to higher Reynolds and Weber numbers, promoting the occurrence of splashing. However, for $\theta = 0.6$, the splashing occurrence decreases from $p = 100\%$ to $p = 64\%$. The crown shows a significant reduction in terms of rim instabilities, presenting a similar development to the isothermal condition. These regimes require further attention, specifically in the spread/splash transition, in order to fully comprehend the underlying mechanisms associated with splashing under non-isothermal conditions.

Table 5 shows the splashing probability for n-heptane under non-splash/splash impact conditions. For isothermal conditions, the spread/splash transition occurs between $U_d = 1.43$ m/s and $U_d = 1.52$ m/s. For $U_d = 1.23$ m/s, the temperature increase is not sufficient to induce splashing, whereas for $U_d = 2.09$ m/s, the splashing regime is maintained for the distinct temperature ranges. For the transition regime ($U_d = 1.52$ m/s and $U_d = 1.68$ m/s), this fluid displays a different behaviour. For lower temperatures ($\theta = 0$ and $\theta = 0.1$), a splashing occurrence percentage close to $p = 100\%$ is verified. Despite this, increasing the temperature to $\theta = 0.2$ leads to the suppression of the splashing phenomenon. For the lower impact velocity, $U_d = 1.52$ m/s, the non-splashing regime extends from $\theta = 0.19$ up to $\theta = 0.59$, shifting back to splashing for a higher liquid film temperature ($\theta = 0.81$). For $U_d = 1.68$ m/s, this transitional field is limited to $\theta = 0.19$ and $\theta = 0.37$, corresponding to a splashing occurrence percentage of $p = 0\%$ and $p = 38.5\%$, respectively. Similar to the previous condition, higher temperatures promote the occurrence of splashing, exhibiting a probability of $p = 100\%$ for $\theta = 0.59$ and $\theta = 0.81$

Figure 6 shows the droplet impact of an n-heptane droplet at different temperatures for $U_d = 1.52$ m/s. For

Table 5 Splashing occurrence percentage as a function of the impact velocity and dimensionless temperature for n-heptane

θ	1.23	1.43	1.52	1.68	2.09
0	**0**	**0**	*90*	*100*	*100*
0.10	**0**	**0**	*80*	*100*	*100*
0.19	**0**	**0**	**0**	**0**	*100*
0.37	**0**	**0**	**0**	***38.5***	*100*
0.59	**0**	**10**	**10**	*100*	*100*
0.81	**0**	*80*	*100*	*100*	*100*

Spreading - Bold, Transition - Bold Italic, Splashing - Italic

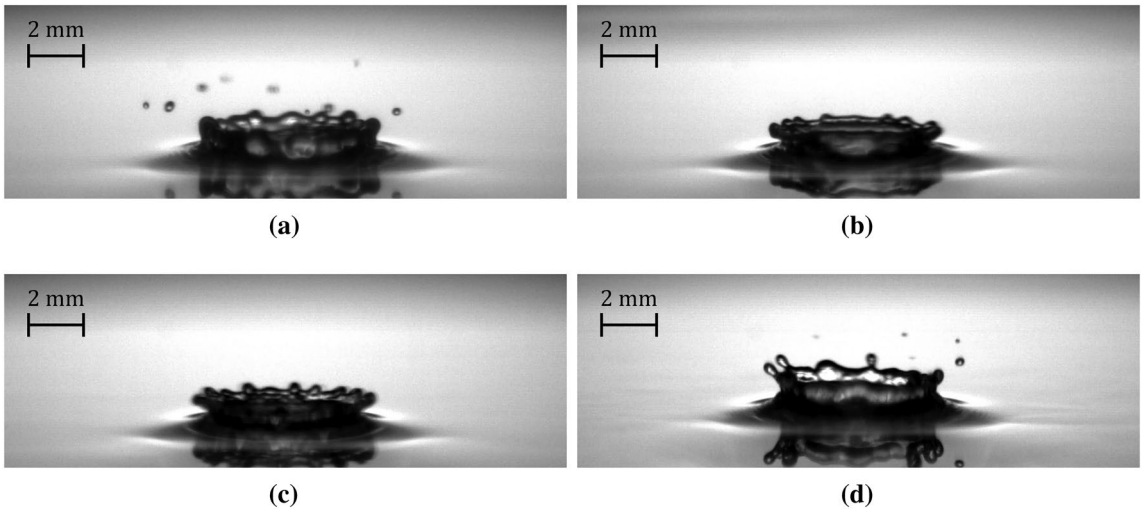

Fig. 6 Visualisation of the impact phenomena of an n-heptane droplet onto a liquid film for different temperatures $\left(U_d = 1.52\ \text{m/s},\ D_d = 2.56\ \text{mm}\right)$: a) $\theta = 0$, $\tau = 1.78$; b) $\theta = 0.19$, $\tau = 1.48$; c) $\theta = 0.37$, $\tau = 1.48$; d) $\theta = 0.81$, $\tau = 1.63$

ambient conditions ($\theta = 0$), the impact outcome is characterised by the formation of a liquid crown and posterior secondary atomisation. The crown displays an irregular rim due to the existence of several cusps, which are the source of secondary droplets. For $\theta = 0.19$, however, the splashing phenomenon is suppressed. The developing crown features several cusps in its rim which do not lead to breakup, contrary to the previous isothermal condition. Increasing the temperature to $\theta = 0.37$ increases the number of cusps in the crown rim, as visible in Fig. 6c, without inducing prompt or crown splashing. Significantly increasing the dimensionless temperature to $\theta = 0.81$ leads to the breakup of these liquid ligaments, producing secondary droplets. This crown displays a more irregular configuration in comparison with lower temperatures. Similarly to water, n-heptane manifests an intermediate region where an increase in the liquid film temperature reduces/suppresses splashing. The liquid film temperature and thermophysical properties play a major role in the impact dynamics, as mainly demonstrated by the splashing occurrence percentages. The transition of spreading to splashing from isothermal to non-isothermal conditions in transitional regimes leads to the existence of temperature-related phenomena that reduce/suppress splashing, such as Marangoni effects. The existence of Marangoni stresses in the contact region of the droplet and the liquid film due to temperature gradients may result in a surface stress imbalance, possibly reducing/suppressing the breakup mechanisms in the crown rim. These regimes where the splashing occurrence is irregular require further research, including transient thermal analysis during impact outcome. This would improve the current knowledge regarding interfacial dynamics under non-isothermal conditions associated with local temperature fluctuations, and heat and mass transfer phenomena.

N-decane displays a similar behaviour to n-heptane, as represented by Table 6. For $U_d = 1.65$ m/s and $U_d = 1.72$ m/s, the lower temperatures are defined by a splashing occurrence of $p = 0\%$. This value tends to increase with higher temperatures, displaying $p = 60\%$ and $p = 20\%$ for $\theta = 0.6$, and $p = 100\%$ for $\theta = 0.82$. This is in accordance to the n-heptane impact condition of $U_d = 1.43$ m/s. In terms of splashing irregularities, these can be observed for $U_d = 1.80$ m/s and $U_d = 2.05$ m/s. Isothermal conditions exhibit a splashing occurrence of $p = 100\%$. An increase in temperature up to $\theta = 0.19$ causes a sudden decrease in secondary atomisation, which is suppressed for $U_d = 1.80$ m/s and reduced for $U_d = 2.05$ m/s. This is limited to $\theta = 0.19$, as higher temperatures revert this effect, which can be visualised in Fig. 7. The crown rims are relatively homogeneous in terms of shape and formation of cusps, whereas the atomisation process varies as a function of the liquid film temperature. Lower temperatures, $\theta = 0$ and $\theta = 0.10$, are characterised by secondary droplets which mostly originate from prompt splashing at earlier stages of the impact. The phenomenon is suppressed for $\theta = 0.2$, as previously mentioned in Table 6, and stabilises for higher temperature conditions. Visually, the secondary droplets exhibit a greater size in comparison with lower temperatures.

In summary, higher liquid film temperatures lead to a substantial decrease in viscosity and surface tension, opposite to density which shows a smaller variation. In terms of percentual variation, viscosity and surface tension exhibit a decrease of 58% and 11% for water, 35% and 23% for n-heptane, and 64% and 36% for n-decane, respectively, from isothermal conditions ($\theta = 0$) up to $\theta = 0.6$. Consequently, this leads

Table 6 Splashing occurrence percentage as a function of the impact velocity and dimensionless temperature for n-decane

θ	1.23	1.43	1.52	1.68	2.09
0	**0**	**0**	*100*	*100*	*100*
0.10	**0**	**0**	*80*	*100*	*90*
0.19	**0**	**0**	**10**	***60***	*100*
0.42	**0**	**0**	**10**	*100*	*100*
0.60	**0**	***60***	**20**	*100*	*100*
0.82	**0**	*80*	*100*	*100*	*100*

Spreading - Bold, Transition - Bold Italic, Splashing - Italic

to higher Weber and Reynolds number, affecting the impact outcomes and correspondent interfacial dynamics associated with splashing/breakup mechanisms. In order to translate the influence of temperature on the splashing phenomenon, these results are contrasted with existing correlations in the literature. For isothermal conditions, the experimental results are in good agreement with the correlation developed by Vander Wal et al. (2006c), which defines the splashing threshold parameter, K, as a function of the Ohnesorge and Reynolds numbers, as represented by Eq. (1):

$$K = OhRe^{1.17} = 63 \tag{1}$$

Despite this, the distinct correlations do not account for temperature differences between the droplet and the liquid film, which is crucial in determining the impact outcomes. In order to properly adapt the Vander Wal et al. correlation, the present work proposes calculating the dimensionless numbers based on the droplet diameter and impact velocity, and the thermophysical properties of the liquid film, which are temperature dependent. This approach is based on the assumption that the liquid film volume is several orders of magnitude higher than the droplet, meaning that the impact phenomena develops at liquid film temperature. Equations 2, 3 and 4 show the adapted Reynolds, Weber and Ohnesorge numbers as a function of both droplet and liquid film properties:

$$Re_{d,f} = D_d U_d \rho_f / \mu_f \tag{2}$$

$$We_{d,f} = D_d U_d^2 \rho_f / \sigma_f \tag{3}$$

$$Oh_{d,f} = \mu_f / \sqrt{\rho_f \sigma_f D_d} \tag{4}$$

The subscripts d and f relate to the droplet and liquid film, respectively. The experimental conditions associated with the adapted dimensionless numbers are displayed in Table 7. The wide range of conditions is obtained through the droplet impact velocity and liquid film temperature variations. Due to the strong dependency of surface tension and viscosity with temperature in comparison with density, the adapted Weber and Reynolds numbers increase for $\theta > 0$. On the contrary, the Ohnesorge number decreases with temperature, meaning that the lower value for this dimensionless number corresponds to $\theta \approx 0.8$. Therefore, isothermal conditions (ambient temperature) correspond to the lower boundaries of the Weber and Reynolds numbers, and to the higher boundary of the Ohnesorge number. This must be evaluated for each fluid and correspondent temperature range.

In order to implement this concept, the correlation proposed by Vander Wal et al. (2006c) is adapted for the current experimental data and is represented by Eq. 5.

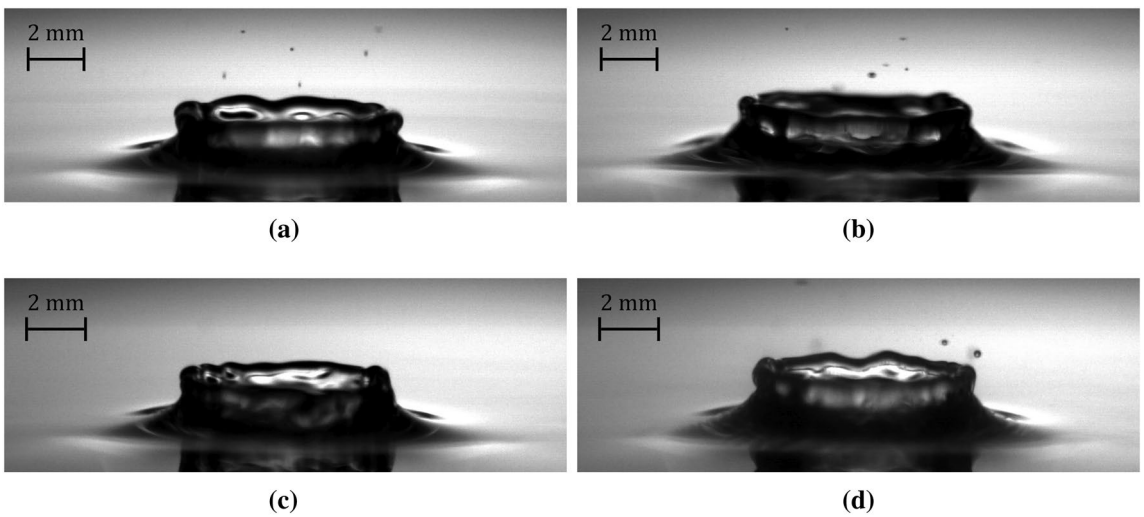

Fig. 7 Visualisation of the impact phenomena of an n-decane droplet onto a liquid film for different temperatures $(U_d = 1.80$ m/s, $D_d = 2.72$ mm$)$: a) $\theta = 0$, $\tau = 6.62$; b) $\theta = 0.10$, $\tau = 7.94$; c) $\theta = 0.19$, $\tau = 5.96$; d) $\theta = 0.37$, $\tau = 6.62$

Table 7 Experimental conditions for the different fluids in terms of adapted Weber, Reynolds and Ohnesorge numbers

Fluid	$We_{d,f}$	$Re_{d,f}$	$Oh_{d,f}$
Water	75 – 304	3807 – 19756	$8.8e-4-2.3e-3$
N-heptane	110 – 502	4820 – 14628	$1.5e-3-2.2e-3$
N-decane	114 – 632	2440 – 14269	$1.8e-3-4.4e-3$

$$K = Oh_{d,f}Re_{d,f}^{1.17} \tag{5}$$

Figure 8 exhibits the adapted correlation for the various experimental results of water, n-heptane and n-decane droplet impact as a function of dimensionless temperature. For visualisation purposes, the solid black symbols refer to spreading, whereas splashing is defined by the open red symbols. Overall, it is possible to identify an increase in the splashing threshold parameter for increasing values of θ. In spite of the dependence of the splashing parameter on the thermophysical properties of the heated liquid film, the spreading and splashing regimes suggest a linear positive pattern with the dimensionless temperature. This tendency is represented by the blue dashed line, which exhibits an apparent segmentation of both regimes, and is expressed by Eq. (6):

$$K = Oh_{d,f}Re_{d,f}^{1.17} = 63(1 + 0.35\theta) \tag{6}$$

For isothermal conditions, $\theta = 0$, the adapted correlation is equal to $K = 63$, which is in conformity with the original correlation developed by Vander Wal et al. (2006c). The highest temperature considered for the experiments, $\theta = 0.82$, leads to an increase of this parameter to $K = 81$. Dimensionless temperatures of $\theta > 0.82$ are not taken into account for the current study, as the liquid film reaches a boiling state. This is characterised by bubble nucleation, growth and possible detachment of vapour bubbles, which will collide with the liquid film interface, inducing instabilities in the form of mechanical waves. This is a distinct regime from the one displayed in Fig. 2, as it involves dynamic liquid films with variable local thickness. The splashing correlation is only applicable for static liquid films with no nucleation sites associated with boiling. In terms of discrepancies, fuels display spreading above the threshold between $\theta \approx 0.2$ and $\theta \approx 0.4$, which corresponds to the transitional regimes in Tables 5 and 6. These results can be displayed in terms of their respective adapted Ohnesorge and Reynolds numbers, as presented in Fig. 9.

The previous proposed correlation is represented by the grey region, where the lower boundary corresponds to $K = 63$ for $\theta = 0$ and the higher boundary to $K = 81$ for $\theta = 0.82$. This region includes experimental data ranging from spreading to splashing for all fluids. N-decane is positioned near the top margin due to high viscosity and low surface tension values, equating to high Ohnesorge numbers. Water demonstrates an opposite behaviour, as high surface tension values lead to lower Ohnesorge numbers, which tend to be located near the lower margin. Overall, the grey area captures the non-splash/splash boundaries effectively. The experimental results may fluctuate depending on the fluids and associated impact conditions. For water, the regime transition from spreading to splashing occurs closer to the lower boundary ($K = 63$), whereas fuels exhibit a higher splashing threshold, mostly due to the transitional regimes between $\theta = 0.2$ and $\theta = 0.4$ ($6000 < Re_{d,f} < 10000$).

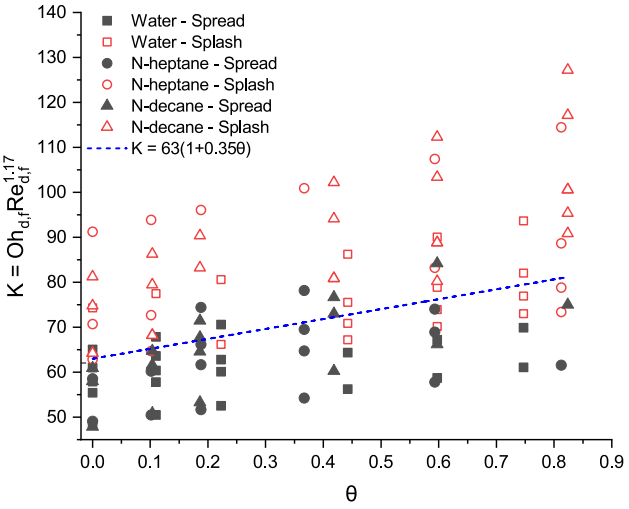

Fig. 8 Adapted splashing threshold parameter, K, as a function of the dimensionless temperature, θ, for the various fluids

To accommodate the experimental results regarding the different fluids and impact conditions, the grey region can be reduced to a single boundary, as revealed by the blue dashed line. This curve, which is a simplification of Eq. (6), is presented by Eq. (7) in the following form:

$$K = Oh_{d,f}Re_{d,f}^{1.17} = 72 \tag{7}$$

In this aspect, the splashing threshold can be calculated in terms of the liquid film thermophysical properties, and the geometrical properties of the droplet. In order to complement the proposed correlations, a separate study focused on transitional regimes should be considered to fully comprehend the role of temperature on the impact dynamics. The suppression of splashing for low temperatures under non-isothermal conditions requires a deep understanding of fluid and heat flow, specifically Marangoni stress and local evaporation. Future work should include heated droplets and liquid films, variable liquid film thickness, and additional fluids with distinct thermophysical properties, which may provide additional insight onto temperature-related phenomena

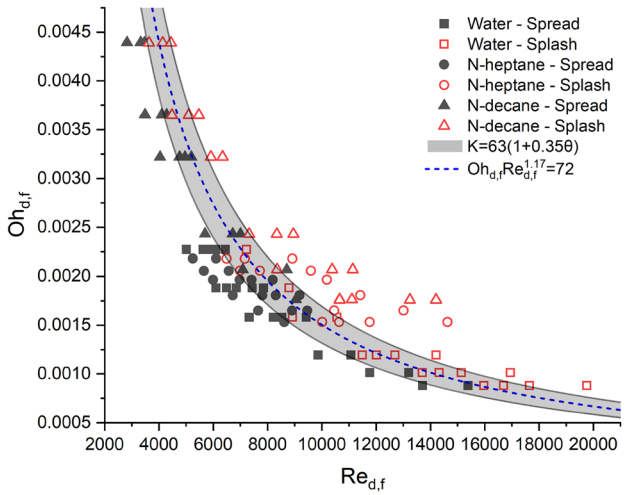

Fig. 9 Splashing evaluation in terms of adapted Ohnesorge and Reynolds numbers for the experimental conditions

associated with non-isothermal impact conditions. The impact of single droplets onto liquid films of different fluids can also be evaluated under isothermal and non-isothermal conditions, however several constraints would arise. These include the dependence of thermophysical properties not only on temperature but also on the mass fraction for each of the fluids. The miscibility of both fluids is also a factor, as miscible/immiscible fluids behave differently in terms of interfacial dynamics. Additionally, differences in saturation temperatures may lead to distinct interactions between fluids, including vapour plume bursting and explosion. The experimental setup is also limited by several factors, including manual weighing processes, optical access difficulties for higher temperature regimes due to increased evaporation, and a maximum operating condition of $T = 250°C$. These require optimisation to extend the scope of the current study.

4 Conclusions

The splashing dynamics were evaluated both qualitative and quantitatively for a broad range of impact velocities and liquid film temperatures. Heated liquid films display an influence in the splashing impact dynamics, affecting the crown development and breakup mechanisms. An increase in the liquid film temperature leads to the transition from spreading to splashing, which is less evident for fuels in comparison with water. In terms of visualisation, this also promotes the formation of cusps on the crown rim, which tend to increase in size and number until rupturing into secondary atomisation. Transitional regimes may display some discrepancies, such as splash suppression/reduction, which is the case for fuels at $\theta = 0.2$ and water at $\theta = 0.6$, respectively. In terms of the splashing threshold, this parameter can be adapted as a function of both the thermophysical properties of the heated liquid film and the dimensionless temperature. The experimental results are in good agreement with the proposed correlations. The general form, $K = Oh_{d,f}Re_{d,f}^{1.17} = 63(1 + 0.35\theta)$, exhibits a positive tendency with the dimensionless temperature, whereas the simplified form, $K = Oh_{d,f}Re_{d,f}^{1.17} = 72$, is based on the thermophysical properties of the liquid film. Improving the existing correlations would require a thorough understanding of interfacial dynamics associated with temperature gradients and phase-change processes.

Appendix A Thermophysical Properties

A.1. N-heptane

Density : $\rho = 0.23237 \times 0.26020^{-(1-T/540.26)^{0.2791}}$

Viscosity : $\log_{10}(\mu) = -5.7782 + 8.0587e2/T + 1.3355e-2T - 1.4794e-5T^2$[mPas]

Surface tension : $\sigma = 53.64(1 - T/540.26)^{1.2431}$[mN/m]

Thermal conductivity : $\log_{10}(k) = -1.8482 + 1.1843(1 - T/536.40)^{2/7}$[W/mK]

Heat capacity : $C_p = 101.121 + 9.7739e-1T - 3.0712e-3T^2 + 4.1844e-6T^3$[J/molK]

A.2. N-decane

Density : $\rho = 0.23276 \times 0.25240^{-(1-T/618.45)^{0.28570}}[\mathrm{g/cm^3}]$

Viscosity : $\log_{10}(\mu) = -6.0716 + 1.0177e3/T + 1.2247e-2T - 1.1892e-5T^2[\mathrm{mPas}]$

Surface tension : $\sigma = 55.777(1 - T/618.45)^{1.3198}[\mathrm{mN/m}]$

Thermal conductivity : $\log_{10}(k) = -1.7768 + 1.0839(1 - T/618.45)^{2/7}[\mathrm{W/mK}]$

Heat capacity : $C_p = 79.741 + 1.6926T - 4.5287e-3T^2 + 4.9769e-6T^3[\mathrm{J/molK}]$

Acknowledgements The present work was performed under the scope of Aeronautics and Astronautics Research Center (AEROG) of the Laboratório Associado em Energia, Transportes e Aeronáutica (LAETA) activities, supported by Fundação para a Ciência e Tecnologia (FCT) through the projects number UIDB/50022/2020, UIDP/50022/2020 and LA/P/0079/2020, and by the Ph.D. scholarship with the reference SFRH BD/143307/2019. It is also supported by "Protocolo celebrado entre a UBI e a Caixa Geral de Depósitos (CGD)" with the reference BAD UBI-CGD 2023/2024 FE.

Author contributions D.V. - Conceptualization, Methodology, Software, Validation, Formal analysis, Investigation, Data Curation, Writing – Original Draft. J.B. - Resources, Writing – Review and Editing, Supervision, Funding acquisition. A.S. - Resources, Writing – Review and Editing, Visualisation, Supervision, Funding acquisition, Project administration.

Funding Open access funding provided by FCT|FCCN (b-on).

Data availability Data is provided within the manuscript.

Declarations

Conflict of interest The authors declare no conflict of interest.

References

Bai C, Gosman A (1995) Development of methodology for spray impingement simulation. SAE Trans. https://doi.org/10.4271/950283

Cossali GE, Coghe A, Marengo M (1997) The impact of a single drop on a wetted solid surface. Experiments Fluids 22(6):463–472

Castillo-Orozco E, Davanlou A, Choudhury PK, Kumar R (2015) Droplet impact on deep liquid pools: Rayleigh jet to formation of secondary droplets. Phys Rev E 92(5):053022

Dinçer İ, Zamfirescu C (2016) Dry Phenom Theory Appl. John Wiley & Sons, New Jersey

Ersoy NE, Eslamian M (2020) Phenomenological study and comparison of droplet impact dynamics on a dry surface, thin liquid film, liquid film and shallow pool. Exp Therm Fluid Sci 112:109977

Farrell J, Cernansky N, Dryer F, Law CK, Friend D, Hergart C, McDavid R, Patel A, Mueller CJ, Pitsch H (2007) Development of an experimental database and kinetic models for surrogate diesel fuels. Technical report, SAE Technical Paper

Foltyn P, Ribeiro D, Silva A, Lamanna G, Weigand B (2021) Influence of wetting behavior on the morphology of droplet impacts onto dry smooth surfaces. Phys Fluids 33(6):063305

Ferrao IA, Silva AR, Moita AS, Mendes MA, Costa MM (2021) Combustion characteristics of a single droplet of hydroprocessed vegetable oil blended with aluminum nanoparticles in a drop tube furnace. Fuel 302:121160

Ferrão I, Vasconcelos D, Ribeiro D, Silva A, Barata J (2020) A study of droplet deformation: the effect of crossflow velocity on jet fuel and biofuel droplets impinging onto a dry smooth surface. Fuel 279:118321

Gao X, Li R (2015) Impact of a single drop on a flowing liquid film. Phys Rev E 92(5):053005

Han Z, Xu Z, Trigui N (2000) Spray/wall interaction models for multidimensional engine simulation. Int J Engine Res 1(1):127–146

Huang Q, Zhang H (2008) A study of different fluid droplets impacting on a liquid film. Pet Sci 5:62–66

Jia W, Qiu H-H (2003) Experimental investigation of droplet dynamics and heat transfer in spray cooling. Exp Thermal Fluid Sci 27(7):829–838

Josserand C, Ray P, Zaleski S (2016) Droplet impact on a thin liquid film: anatomy of the splash. J Fluid Mech 802:775–805

Le M, El Sayah Z, Benrabah R, Warth V, Glaude P-A, Privat R, Fournet R, Sirjean B (2023) An experimental and detailed kinetic modeling of the thermal oxidation stability of n-decane as a jet fuel surrogate component. Fuel 342:127754

Liang G, Guo Y, Shen S (2014) Gas properties on crown behavior and drop coalescence. Numer Heat Transf, Part B Fundam 65(6):537–553

Liang G, Zhang T, Chen Y, Chen L, Shen S (2019) Two-phase heat transfer of multi-droplet impact on liquid film. Int J Heat Mass Transf 139:832–847

Moreira A, Moita A, Panao M (2010) Advances and challenges in explaining fuel spray impingement: how much of single droplet impact research is useful? Progress Energy Combust Sci 36(5):554–580

Mundo C, Sommerfeld M, Tropea C (1995) Droplet-wall collisions: experimental studies of the deformation and breakup process. Int J Multiph Flow 21(2):151–173

Manzello SL, Yang JC (2002) An experimental study of a water droplet impinging on a liquid surface. Exp Fluids 32(5):580–589

Okawa T, Kubo K, Kawai K, Kitabayashi S (2021) Experiments on splashing thresholds during single-drop impact onto a quiescent liquid film. Exp Thermal Fluid Sci 121:110279

Okawa T, Shiraishi T, Mori T (2006) Production of secondary drops during the single water drop impact onto a plane water surface. Exp Fluids 41:965–974

Plateau JAF (1873) Statique Expérimentale et Théorique des Liquides Soumis aux Seules Forces Moléculaires, vol 2. Gauthier-Villars, Paris

Panão MR, Moreira ALN (2005) Flow characteristics of spray impingement in pfi injection systems. Exp Fluids 39:364–374

Rayleigh L (1879) On the capillary phenomena of jets. Proc R Soc London 29(196–199):71–97

Rioboo R, Bauthier C, Conti J, Voue M, De Coninck J (2003) Experimental investigation of splash and crown formation during single drop impact on wetted surfaces. Exp Fluids 35:648–652

Raza M, Mao Y, Yu L, Lu X (2019) Insights into the effects of mechanism reduction on the performance of n-decane and its ability to act as a single-component surrogate for jet fuels. Energy Fuels 33(8):7778–7790

Ribeiro DF, Panão MR, Barata JM, Silva AR (2023) Insights on bubble encapsulation after drop impact on thin liquid films. Int J Multiph Flow 164:104450

Šikalo Š, Ganić E (2006) Phenomena of droplet-surface interactions. Exp Thermal Fluid Sci 31(2):97–110

Selvam RP, Lin L, Ponnappan R (2006) Direct simulation of spray cooling: effect of vapor bubble growth and liquid droplet impact on heat transfer. Int J Heat Mass Transf 49(23–24):4265–4278

Tropea C, Marengo M (1999) The impact of drops on walls and films. Multiph Sci Technol. https://doi.org/10.1615/MultScienTechn.v11.i1.20

Van Dam DB, Le Clerc C (2004) Experimental study of the impact of an ink-jet printed droplet on a solid substrate. Phys Fluids 16(9):3403–3414

Vasconcelos DA, Silva AR, Barata JM (2023) The impact of temperature on heated liquid films: crater and jetting impact dynamics. Exp Therm Fluid Sci 147:110944

Vasconcelos D, Silva A, Barata J (2024) Influence of bubble growth and liquid film instabilities on droplet impact phenomena under saturated boiling regimes. Atomization Sprays 34(4):1–13

Vander Wal RL, Berger GM, Mozes SD (2006) The combined influence of a rough surface and thin fluid film upon the splashing threshold and splash dynamics of a droplet impacting onto them. Exp Fluids 40(1):23–32

Vander Wal RL, Berger GM, Mozes SD (2006) Droplets splashing upon films of the same fluid of various depths. Exp Fluids 40(1):33–52

Vander Wal RL, Berger GM, Mozes SD (2006) The splash/non-splash boundary upon a dry surface and thin fluid film. Exp Fluids 40(1):53–59

Wang A-B, Chen C-C (2000) Splashing impact of a single drop onto very thin liquid films. Phys Fluids 12(9):2155–2158

Yarin AL (2006) Drop impact dynamics: splashing, spreading, receding, bouncing. Annu Rev Fluid Mech 38:159–192

Yaws CL (1999) Chemical properties handbook. McGraw-Hill Education, New York

Yu X, Shao Y, Teh K-Y, Hung DL (2022) Force of droplet impact on thin liquid films. Phys Fluids 34(4):042111

Yarin AL, Weiss DA (1995) Impact of drops on solid surfaces: self-similar capillary waves, and splashing as a new type of kinematic discontinuity. J Fluid Mech 283:141–173

Zhu J, Tu C, Lu T, Luo Y, Zhang K, Chen X (2021) Behavior of a water droplet impacting a thin water film. Exp Fluids 62:1–13